Molecular Crystals and Liquid Crystals

Publication details, including instructions for authors and subscription information:
http://www.tandfonline.com/loi/gmcl20

Chaotic Rotations Generated by Light in Nematic Liquid Crystals

E. Brasselet [a] & L. J. Dubé [b]

[a] Laboratoire de Physique UMR 5672, École Normale Supérieure de Lyon, Lyon Cedex, France

[b] Département de Physique, de Génie Physique, et d'Optique, Université Laval, Cité Universitaire, Québec, Canada*

Version of record first published: 22 Sep 2006

To cite this article: E. Brasselet & L. J. Dubé (2006): Chaotic Rotations Generated by Light in Nematic Liquid Crystals, Molecular Crystals and Liquid Crystals, 453:1, 93-105

To link to this article: http://dx.doi.org/10.1080/15421400600651716

Mol. Cryst. Liq. Cryst., Vol. 453, pp. 93–105, 2006

ISSN: 1542-1406 print/1563-5287 online
DOI: 10.1080/15421400600651716

Taylor & Francis
Taylor & Francis Group

Chaotic Rotations Generated by Light in Nematic Liquid Crystals

E. Brasselet
Laboratoire de Physique UMR 5672, École Normale Supérieure de Lyon, Lyon Cedex, France

L. J. Dubé
Département de Physique, de Génie Physique, et d'Optique, Université Laval, Cité Universitaire, Québec, Canada*

Various nonlinear rotation regimes are observed in an optically excited nematic liquid crystal film under boundary conditions (for the light and the material) that are invariant by rotation. Th excitation light is circularly polarized, the intensity profile is circularly symmetric and the beam diameter at the sample location is a few times smaller than the cell thickness. A transition to chaos via quasiperiodicity is identified when the light intensity is taken as the control parameter. Transverse nonlocal effects are suggested to be the cause of the observed dynamics and a simple model consisting of a collection of coupled rotators is developed to provide a qualitative explanation.

Keywords: chaotic rotations; optically induced dynamics; time series analysis; transverse nonlocal effects

I. INTRODUCTION

The long-range orientational order of the molecules in liquid crystals adds a collective character to the light-matter interaction and generates a unique spatiotemporal feedback mechanism responsible for the dynamical richness of the optically induced orientational phenomena.

We would like to thank T. V. Gasltian for the access to his experimental facilities at the Center for Optics and Laser, Laval University, Québec, Canada.

*Also at Laboratoire de Chimie-Physique-Matière et Rayonnement, Université Pierre et Marie Curie, Paris, France.

Address correspondence to Etienne Brasselet, Laboratoire de Physique UMR 5672, École Normale Supérieure de Lyon, 46 Allée d'Italie, 69364 Lyon Cedex 07, France. E-mail: ebrassel@ens-lyon.fr

This is particularly true when the light-matter system is not invariant under rotation around the light propagation axis (e.g. elliptical polarization [1], asymmetric intensity profile at normal incidence [2] or ordinary waves at small oblique incidence [21]), where quasi-periodic or chaotic behavior have already been reported [1,2]. Such systems are not only interesting by themselves but can be viewed as suitable candidates to test experimentally generic sets of equations describing nonlinear dynamics.

For instance, chaotic rotations have retained much attention in the context of the phase synchronization of coupled chaotic oscillators [3,4] and in the study of chaotic bounded flows [5]. Since the dynamics of a number of well-known systems can be reduced to a chaotic rotation (e.g., the Rössler and the Lorenz systems), the study of real systems that exhibit chaotic rotations is of special interest. Quite recently, chaotic rotations generated by light in a nematic liquid crystal (NLC) film has been observed [2]. The light was circularly polarized with an astigmatic intensity profile and the existence of a chaotic rotation of the director (i.e., the unit vector $\boldsymbol{n}$ that defines the local orientation of the optical axis of the NLC) has been ascribed to the rotational asymmetry arising from the astigmatism of the excitation beam [2].

In the present contribution, we show that complex and intriguing reorientation dynamics can also be generated in the presence of rotational invariance. The interaction geometry corresponds to a light beam with circular polarization and circularly symmetric intensity profile focused on a homeotropic nematic liquid crystal film. The director trajectory is reconstructed solely from the experimental data obtained from the analysis of the light at the output of the sample. We observe the following sequence of distinct dynamical regimes when the light intensity, taken as the control parameter, is increased: periodic, quasiperiodic, chaotic, quasiperiodic, periodic. The appearance of this scenario is ascribed to the use of a beam diameter a few times smaller than the cell thickness. The competition between finite beam size effects and spin angular momentum transfer to the medium will also be discussed.

II. EXPERIMENTS AND TIME SERIES ANALYSIS

A. Experimental Procedure and Dynamical Scenario

Our observations concern a homeotropically aligned NLC cell illuminated by a circularly polarized laser beam operating at 532 nm in the fundamental mode TEM_{00} whose Gaussian intensity profile is written $I(x,y) = I_0 \exp[-2(x^2 + y^2)/w_0^2]$. The light beam is focused on the sample by means of a lens with focal length 150 mm at normal

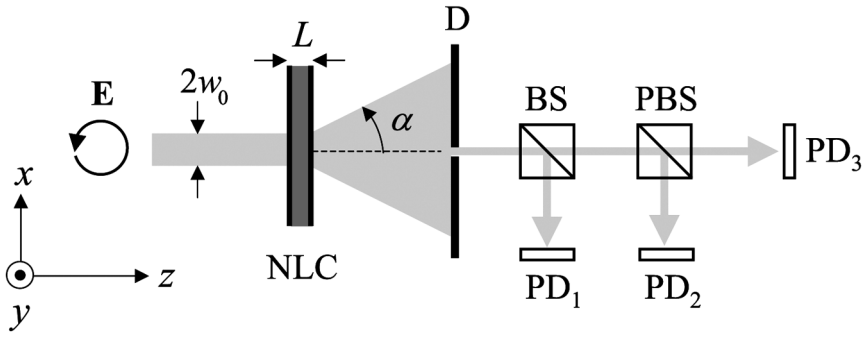

FIGURE 1 Sketch of the experimental set-up. $2w_0$ is the beam diameter defined at e^{-2} of its maximal intensity; **E**, circularly polarized incident electric field; NLC, nematic liquid crystal film of thickness L; D, diaphragm; BS, beamsplitter; PBS, polarization beamsplitter; PD_i, photodiodes. The angle α is the divergence angle of the beam after its passage through the reoriented film resulting from self-focusing effects. This angle may be tens of degrees in the strongly reoriented states ($\Theta_{\max} \simeq 1$). The photodiode PD_1 collects the intensity I_c, which is proportional to the total intensity emerging from the diaphragm and $PD_{2,3}$ collect the intensities $I_{x,y}$ of the horizontal and vertical component of the electric field.

incidence (along the z-axis). The beam diameter $2w_0$, at e^{-2} of maximum intensity at the sample location, is measured to be 30 μm and the cell thickness is $L = 75\,\mu m$. The experimental set-up is shown in Figure 1. It permits the monitoring of the director dynamics via the real-time acquisition of the total intensity I_c of the central part of the emerging excitation beam (placing a diaphragm at the output of the sample) and the intensities of the horizontal and vertical components of the electric field, I_x and I_y ($I_c = I_x + I_y$). This set-up has been originally used in a previous study [6] where it is explained that there are the following relationship between the time series and the angles that define the director: $I_c \leftrightarrow \Theta$ and $i \leftrightarrow \Phi$, where $i \equiv I_x/I_c$ and the director $\boldsymbol{n} = (\sin\Theta\cos\Phi, \sin\Theta\sin\Phi, \cos\Theta)$.

In the present work we propose to reconstruct the director trajectory in the (x,y) plane solely from the experimental quantities $I_c(t)$ and $i(t)$. For this purpose, we define a mathematical object $(\widetilde{n}_x, \widetilde{n}_y) = (\widetilde{n}_\perp \cos\widetilde{\Phi}, \widetilde{n}_\perp \sin\widetilde{\Phi})$ which embodies the dynamics of the physical director. We choose

$$\widetilde{n}_\perp(t) = I_c(t), \tag{1}$$

whereas the azimuthal degree of freedom $\widetilde{\Phi}$ is reconstructed from the time series $i(t)$. First, we calculate the time delay τ_d that corresponds

to the first zero of the auto-correlation function $C(f,\tau) = T^{-1}\int_0^T f(t)\times f(t+\tau)dt$ where T is the duration of the time series $f(t)$ (in practice we used the zer-mean-value of f(t)). Then $\widetilde{\Phi}$ is defined as

$$\widetilde{\Phi}(t) = \arctan\left[\frac{i(t+\tau_d)}{i(t)}\right]. \tag{2}$$

The excitation intensity is progressively increased starting from the unperturbed state [i.e. $\rho < 1$ where $\rho = I/I_F$ is the light intensity I normalized to the optical Fréedericksz transition threshold value I_F]. The sampling time is $\Delta t = 0.25$ s, which is more than one order of magnitude smaller than the characteristic reorientation time of the cell estimated to be $\tau_{\mathrm{NLC}} \simeq 5$ s. The complete experiment lasted up to 20 hours without anchoring breakdown, which enables data acquisition during several hours for each value of the intensity, at a fixed point of the sample. Time series with duration 10^4 s have then been extracted for each regime to plot the director trajectories in the plane $(\widetilde{n}_x, \widetilde{n}_y)$, which are shown in Figure 2. In fact, the long-term behavior of the azimuthal angle is always a quasi-uniform precession around the light propagation axis (z), and one can write

$$\widetilde{\Phi}(t) = \Omega t + \Psi(t). \tag{3}$$

The angular velocity Ω corresponds to a long-term uniform precession of the director around the z-axis whereas $\Psi(t)$ describes the non-uniform part of the azimuthal dynamics. The director dynamics amounts therefore to nonlinear rotations and the observed five disctinct regimes are labeled Rn ($n = 1, 2, 3, 4$ and 5) for intensities $\rho = 1.10, 1.31, 1.53, 1.63$ and 1.72 respectively. The Figure 2 shows these different director trajectories in red, for typical temporal windows of duration $2\pi/\Omega$. The regimes R1, R2 and R3 correspond to small

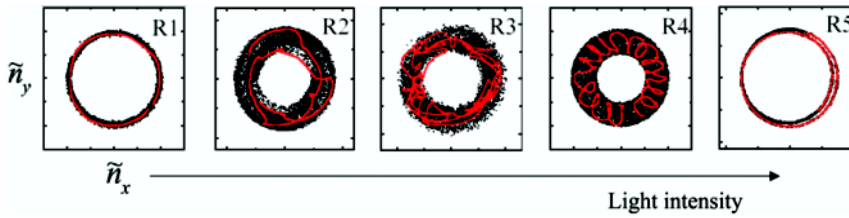

FIGURE 2 Experimental director trajectory in the $(\widetilde{n}_x, \widetilde{n}_y)$ plane. (a) R1 at $\rho = 1.10$; (b) R2 at $\rho = 1.31$; (c) R3 at $\rho = 1.53$; (d) R4 at $\rho = 1.63$; (e) R5 at $\rho = 1.72$. Trajectories for a short temporal window appear in red.

reorientation amplitude (i.e. the maximum reorientation amplitude $\Theta_{\max}$ satisfies $\Theta_{\max}^2 \ll 1$), where only one self-diffraction ring [7] is observed at the maximum with $\Theta_{\max} \simeq 0.2$. In contrast, the regimes R4 and R5 exhibit several rings (up to 20) and correspond to strongly reoriented states ($\Theta_{\max} \simeq 1$).

The observed sequence of regimes differs from the one predicted by infinite plane wave (IPW) model where instead a sequence of type R1 $\rightarrow$ R2 $\rightarrow$ R5 is predicted [8]. The unexpected regimes R3 and R4 can thus be attributed at first sight to finite beam size effects as suggested by our preliminary observations [6]. We will next characterize the sequence of nonlinear rotations Rn with a detailed (linear and nonlinear) time-series analysis.

B. Data Analysis

1. Linear Measures

We have selected three linear indicators to begin the analysis of the time series, namely the evaluation of Ω (which is obtained by fitting $\widetilde{\Phi}(t)$ to a linear function), the auto-correlation function and the Fourier power spectrum for the time series $I_c(t)$ and $i(t)$ for each rotating regime Rn ($n = 1, 2, 3, 4$ and 5). From Table I, we see that the averaged precession rate Ω is a decreasing function of n, which indicates that the averaged reorientation angle Θ increases with intensity (the viscous torque scales as $\sin^2\Theta$). The almost periodic rotating regimes R1 and R5 thus differs only by their characteristic time scale, the precession rate of R5 being approximately 20 times smaller than that of R1. In distinction, a nutation motion [$\partial_t\Theta \neq 0$] is coupled to precession for the R2, R3 and R4 regimes, as indicated by a thickening of the trajectory in the (x, y) plane. Obviously, these three regimes are qualitatively different: the regime R3 looks particularly irregular whereas

TABLE I Linear and Nonlinear Dynamical Characteristics of the Rotating Regimes R1, R2, R3, R4 and R5: Angular Velocity Ω, Auto-correlation Times τ_c of the Time Series $I_c(t)$ and $i(t)$ and Converged Correlation Dimension $\overline{d}_2$.

Regime	Ω(deg/s)	$\tau_c[I_c]$(s)	$\tau_c[i]$(s)	$\overline{d}_2$	Nature
R1	19.1	—	5100	1.16 ± 0.13	periodic
R2	13.8	160	810	1.99 ± 0.07	quasi-periodic
R3	13.1	12	400	2.22 ± 0.17	chaotic
R4	7.56	200	7800	1.47 ± 0.04	quasi-periodic
R5	0.91	—	—	—	periodic

the regime R2 and R4 exhibit a rather quasi-periodic precession-nutation motion of the director.

The auto-correlation functions $C(f,\tau)$ of the sequences R2, R3 and R4 reveal further distinctive features of the three regimes. For instance, they are each characterized by a distinct pair of auto-correlation times $\{\tau_c[i],\tau_c[I_c]\}$ (Table I) where $\tau_c[f]$ is estimated as the time when the envelope of $C(f,\tau)$ has fallen by a factor 10. The sudden decrease of $\tau_c[\mathrm{I_c}]$ as one goes from R2 to R3 indicates that a drastic broadening must have occurred in the Fourier spectrum of $I_c(t)$ associated with the appearance of new frequencies. This has been confirmed with the power Fourier spectra of the regimes R2, R3 and R4. We have found a relatively important contribution of low frequencies in the R3 regime suggesting that a transition to a very irregular regime (still to be characterized) has occurred between R2 and R3. This low frequency background disappears at higher intensity (R4 regime) and demonstrates the intrinsic nonlinear nature of the R3 dynamics. This also rules out the appearance of an experimental noise caused by the irreversible degradation of the anchoring condition and of the integrity of the nematic film.

To get a further grasp on the characteristics of the different regimes, and especially to identify the complex R3 dynamics as chaos, we now turn to the tools of nonlinear analysis.

2. Nonlinear Measures

Although visual irregularity and spectral broadening are necessary indices for the presence of chaotic dynamics, they are not sufficient to distinguish a complicated signal from a chaotic one. The nonlinear analysis toolbox has matured considerably during the past decades [9] and some of the methods are becoming standard and useful when employed wih the necessary care.

In order to quantify the complexity of the system, we build from the scalar time series $\{x_j, j=1,2,\ldots,N\}$ ($x_j = x(j\Delta t)$ where Δt is the sampling time), a set of time-delay vectors $\mathbf{X}_j = \left(x_j, x_{j+n_d}, \ldots, x_{j+(d_E-1)n_d}\right)$ with $\tau_d = n_d\Delta t$ in a reconstructed state space of embedding dimension d_E. The vectors $\mathbf{X}_j$ can then be used to calculate a dimension estimate via the correlation sum $C_2(\mathbf{X},\epsilon)$ whose practical implementation follows Ref. [9]. The correlation sum is simply the fraction of all possible pairs of points which are closer than a given distance ϵ in a particular norm. In the limit of an infinite amount of data ($N\to\infty$) and for small ϵ, we expect C_2 to scale as $C_2(\mathbf{X},\epsilon)\propto\epsilon^{d_2}$ thereby defining the correlation dimension d_2. In practice, d_2 is obtained on a log-log plot as the slope of C_2 versus ϵ within the scaling range. We have carried

out the calculations of these estimates for the different regimes and for the sequences $i(t)$ and $I_c(t)$ in embedding dimensions $d_E = 1, \ldots, 7$.

The calculations on the original data have indicated that the correlation dimension d_2 keeps increasing with embedding dimension d_E. This behavior is not specific to any particular regimes nor to the choice of the sequence (I_c or i) and is traceable to the presence of noise in the data invading the higher dimensions of the underlying lower dimensional system. At this point, no reliable estimate of d_2 can be given.

We have then applied a nonlinear noise-reduction algorithm to the original data. For our purpose, a few experimentations have shown the simplest noise-reduction method proposed by Schreiber [10] to be quite effective. It consists basically in the replacement of $\mathbf{X}_i$ by an average over its neighbors, i.e. $\mathbf{X}_i \to \widetilde{\mathbf{X}}_i = (1/N_i(\epsilon)) \sum_{j=1}^{N_i(\epsilon)} \mathbf{X}_j$ where $N_i(\epsilon)$ is the number of neighbors of $\mathbf{X}_i$ within a distance ϵ. As an example, the resulting noise-reduced data for the regime R2 appear in Figure 3(b,d) where the main features are nicely sharpened as qualitative indicator of the noise reduction. The success of the operation is also gauged by an enlarged scaling region of the correlation sum. The dimension calculations have been repeated on the noise-reduced data with a scaling range extending over two orders of magnitude where we

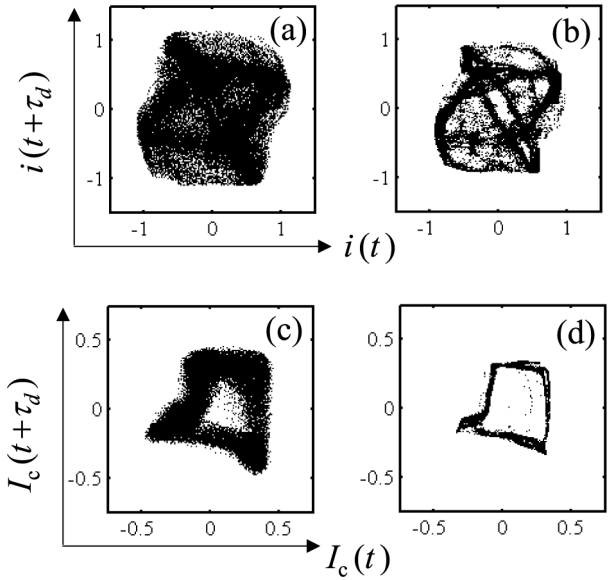

FIGURE 3 Reconstructed phase space $i(t + \tau_d)$ versus $i(t)$ (a,b) and $I_c(t + \tau_d)$ versus $I_c(t)$ (c,d) of the regime R2. (a,c) original data; (b,d) noise-reduced data.

have found that the correlation dimension d_2 now saturates rapidly as a function of d_E.

Our dimension results for all 4 regimes of the noise-reduced sequence $i(t)$ appear in the Table I where the average correlation dimension $\overline{d}_2$ is tabulated for R1 and R4 (R2 and R3) the average is taken over $2 \leq d_E \leq 7$ $(3 \leq d_E \leq 7)$ and the error bars indicate the standard deviation about the mean. Thus far, it is safe to attribute the label quasi-periodic for the regimes R2 ($\overline{d}_2 \simeq 2.0$) and R4 ($\overline{d}_2 \simeq 1.5$). In contrast, a further quantitative measure is needed to classify R3 ($\overline{d}_2 \simeq 2.2$).

Possibly the best evidence for chaos is a positive Lyapunov exponent. If $\mathbf{X}(t)$ is the time evolution of some initial condition $\mathbf{X}(0)$ in the appropriate phase space, the largest Lyapunov exponent $\lambda_{\max}$ is found with probability one by $\lambda_{\max} = \lim_{t\to\infty} \lim_{\epsilon\to 0}[(1/t) \ln (||\mathbf{X}(t) - \mathbf{X}_\epsilon(t)||/\epsilon)]$ with $||\mathbf{X}(0) - \mathbf{X}_\epsilon(0)|| = \epsilon$. As estimator, we have implemented the algorithm introduced by Rosenstein *et al.* [11] and Kantz [12]. We find for R3, $\lambda_{\max} \simeq 0.18\,\mathrm{s}^{-1}$. This value should however be compared with that of the most periodic sequence, namely that of $i(t)$ in the R1 regime, which should set a reference value, λ_0, ideally equal to zero. We obtain $\lambda_0 \simeq 4 \times 10^{-3}\,\mathrm{s}^{-1}$, two orders of magnitude smaller than that of the R3 regime. This conclusively identifies R3 as a chaotic regime.

III. DISCUSSION

A. Comparison with Previous Studies

They are very few reported cases of optically induced chaotic oscillations in NLC. One example is the case of an s-polarized laser beam at small incidence angle [13,14]. "In this geometry, a recent numerical analysis succeeded to recover all the qualitative experimental features of the dynamics [21]". Another is the situation of a circularly polarized light beam at normal incidence having an asymmetric intensity profile [2]. Finally, irregular oscillations have also been observed in the case of a linearly polarized light beam at normal incidence with an elliptical intensity profile whose major axis is orthogonal to the electric field's direction [15]. However no quantitative characterization of possible chaoticity is available in this latter case. We have collected the results in Table II for comparison. The transition to chaos still poses a challenge to a theoretical description since none of the compiled results, including ours, can be explained at present with the available models.

There are striking similarities however between our results and those of Vella *et al.* [2] concerning the regime of chaotic rotations by comparing the graphs related to R3 in Figure 2 and Figure 1(a,c,d) of Ref. [2]. Obviously the interaction geometries are different: only

TABLE II Comparison of the Chaotic Rotation Regime R3 to Other Studies where Chaotic Dynamics of the Director has been Observed. λ_0 is the Maximal Lyapunov Exponent in the Fundamental Periodic Regime (R1 in Our Case), $\lambda_{\max}$ is the Maximal Lyapunov Exponent in the Chaotic Regime (R3 in Our Case) and $\overline{d}_2$ the Converged Value of the Correlation Dimension. When the Parameter $\delta = 2w_0/L$ is Multivalued, the Values Correspond to its Minimum and Maximum Respectively. An Empty Entry Indicates that the Corresponding Information is not Available.

Reference	Polarization	Beam shape	δ	$\lambda_0(\tau_{\mathrm{NLC}}^{-1})$	$\lambda_{\max}(\tau_{\mathrm{NLC}}^{-1})$	$\overline{d}_2$
[13]	oblique *o*-wave	circular	1	2.5×10^{-3}	≥ 0.2	3.35
[14]	oblique *o*-wave	circular	0.93	5.6×10^{-5}	5.6×10^{-3}	—
[2]	circular	elliptical	0.32/3.2	2.5×10^{-3}	$\geq 8.2\times10^{-3}$	3.50 ± 0.05
Present work	circular	circular	0.4	2.3×10^{-2}	1.03	2.22 ± 0.17

the spin part of angular momentum of the incident photons is involved in the present work whereas both orbital and spin angular momenta play a role when complex dynamics is observed in Ref. [2]. There, the pure spin case corresponds to ratios $\delta_{x,y} = 2w_{x,y}/L = 3.2$ and the spin-orbital case corresponds to ratios $\delta_x = 0.32$ and $\delta_y = 3.2$. Vella *et al.* [2] concluded that the complexity arises from the competition between the orbital and the spin angular momentum of light. However our results, obtained with $\delta_{x,y} = 0.4$, do not involve the orbital part of the angular momentum of light and invite the reconsideration of the interpretation given in Ref. [2]. In addition, the parameter δ has already been identified to gauge the finite size effects on the reorientation dynamics [6,16]. Therefore we believe that the results of Ref. [2] could be attributed, at least in part, to finite beam size effects rather than a competition between the spin and the orbital components of the light angular momentum.

In the next section, we derive a simple model that emphasizes the role of transverse nonlocal effects in the optically induced reorientation dynamics of NLC under light beam of finite extent. It will be shown that the parameter δ can indeed be viewed as a suitable control parameter and we determine the existence of a critical value δ_c under which the dynamics is much enriched.

B. A Kuramoto-like Model

The experiments have implicitly revealed the existence of a characteristic value δ_c below which dynamical regimes occur that have no

counterpart in the infinite plane wave limit. The situation can be qualitatively analyzed with the introduction of the electric coherence length estimated at the Fréedericksz threshold intensity I_F, namely $\xi(\delta) = \xi^{\mathrm{IPW}}/(1+\overline{\delta}/\delta)$, where ξ^{IPW} is the coherence length in the IPW limit. This equation defines an intrinsic δ, $\overline{\delta} = 2^{3/2}/\pi \simeq 0.90$ below which transverse nonlocal effects should be important and therefore identifies $\overline{\delta}$ as a relevant estimation of the critical value δ_c referred to previously.

Our goal here is to extract the essential features of transverse nonlocal dynamical effects and to reduce the initial problem (a set of coupled partial differential equations involving all space coordinates and time) to a finite set of ordinary differential equations with respect to time. This can be achieved by the discretization procedure sketched in Figure 4 where w_0 and w_Θ are the radii (at e^{-2}) of the light intensity and the reorientation profiles respectively. The actual reorientation profile is not known and will not be calculated: it is assumed as a first guess to behave as $\Theta = \Theta_{\max} e^{-2r^2/w_\Theta^2} \sin(\pi z/L)$ where $r^2 = x^2 + y^2$, $\Theta_{\max}$ is the amplitude of the lowest reorientation mode estimated at $r = 0$ and the radius w_Θ is expressed as $w_\Theta = L(2^{1/2}\delta/\pi)^{1/2}$ as first derived in Ref. [17]. We then reduce the initial problem to a one-dimensional finite assembly of rotators (excited via light-matter spin angular momentum exchanges) at locations $r_i = i\xi$ where i is an integer running from $-N$ to N, with N defined as the integer part of

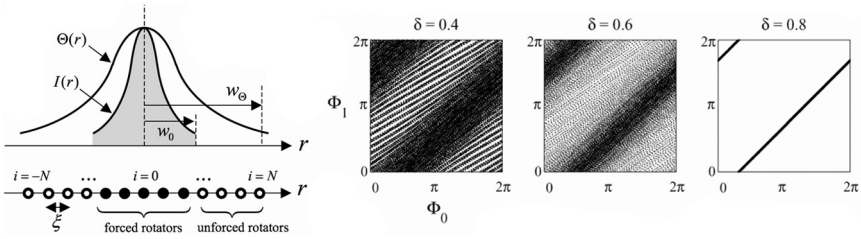

FIGURE 4 Left part: Reduction of the initial problem, where the light intensity profile $I(r)$ and the reorientation profile $\Theta(r)$ have respectively a spatial extension w_0 and w_Θ, to a unidimensional finite set of rotators equally spaced by the distance ξ. Typically, the rotators located under the Gaussian light excitation ($r_i < w_0$) are forced (filled circles) by light angular momentum deposition to the medium while those located beyond w_0 are considered unforced (open circles). Right part: Phase diagram Φ_1 as a function of Φ_0 for $\delta = 0.4$, 0.6 and 0.8. Phase locking occurs at $\delta_c \simeq 0.7$. The normalized integration time is 500 times the period of the rotator located at $r = 0$, the initial conditions are $\Phi_i = 0$ for all i and the transient has been removed. In each case, the total number of rotators is $2N + 1 = 9$.

the ratio w_Θ/ξ (Fig. 4). The reduced system consists of $2N+1$ coupled rotators represented by the pair of angles (Θ_i, Φ_i). By restricting the dynamics of the rotators to their simplest form by imposing fixed polar angles and by ignoring any twisted modes of reorientation, we obtain a set of coupled differential equations of the form [18].

$$\frac{\partial \Phi_i}{\partial \tau} = \omega_i + \sum_{j \neq i} \Gamma_{ij}(\delta, \Theta_i, \Theta_j) \sin(\Phi_j - \Phi_i). \tag{4}$$

The simulations have been done with the material parameters $\epsilon_{||_{1/2}} = 1.75$ and $\epsilon_{\perp_{1/2}} = 1.52$ corresponding to the NLC material E7 (from Merck datasheet) and taking for initial conditions $\Phi(\tau = 0) = 0$ for all i. For the purpose of demonstration, we focus our attention to the dynamics of the rotators located in the central part of the excitation beam, namely $i = 0$ and $i = \pm 1$ by looking at the behavior of Φ_1 as function of Φ_0 [the dynamics for $i = -1$ and $i = 1$ are identical]. The results are shown in Figure 4 where the phase diagrams have been plotted for $\delta = 0.4$, 0.6 and 0.8. Above $\delta = 0.8$ the situation is qualitatively unchanged with respect to the case $\delta = 0.8$, i.e., a phase-locked regime is observed. Therefore Figure 4 illustrates the existence of a critical value $\delta_c \simeq 0.7$ that separates two distinct dynamics. For $\delta > \delta_c$ the central rotators are phase locked while for $\delta < \delta_c$ they are not. These results clearly indicates that a bifurcation has occured at $\delta = \delta_c$, which is a generic behavior for coupled oscillators. Despite the fact that the proposed modelization is based on reasonable physical arguments, it remains somewhat too simple a model. It consists of a collection of pure phase oscillators while the experiments correspond to both phase (Φ) and amplitude (Θ) dynamics. Nevertheless, the critical value $\delta_c \simeq 0.7$ matches approximately the distinctive value $\overline{\delta} \simeq 0.90$ that appears in the expression of the coherence length and agrees with the observations. Therefore, when δ is sufficiently small, the observation of new dynamical regimes (e.g., the regimes R3 and R4, new with respect to the IPW limit) appear directly as manifestations of transverse nonlocal effects.

IV. CONCLUSION

We have proposed an experimental method for the reconstruction of the director reorientation dynamics when a nematic liquid crystal film is excited by light. We have demonstrated that a novel sequence of nonlinear rotations of the type "periodic → quasi-periodic → chaotic → quasi-periodic → periodic" takes place when the excitation beam is circularly polarized with a symmetric intensity profile. This

bifurcation scenario is only observed when the beam diameter is sufficiently small compared to the cell thickness and is not predicted by available theoretical models.

It may be interesting to note that the system of equations (4) has the generic form of the well-known model of Kuramoto [19] (finite dimensional in our case), which was originally introduced to describe oscillatory chemical reactions. Although the present model can claim only to give a first simple (pure phase oscillators) picture of dynamical transverse nonlocal effects in optically excited NLC films, some results on the collective behavior of limit-cycle oscillators encourage us to include amplitude dynamics in our approach. For instance, Matthews and Strogatz [20] have shown that linearly coupled oscillators with amplitude and phase degrees of freedom near a Hopf bifurcation exhibit unsteady dynamics (i.e., large amplitude oscillations, quasi-periodicity, chaos) in well-defined regions of the coupling strength and a spread of the natural frequencies. In our context, this should be associated with the observation of the chaotic regime, R3, and the quasi-periodic regime with large amplitude oscillations, R4.

REFERENCES

[1] Krimer, D. O., Kramer, L., Brasselet, E., Galstian, T. V., & Dubé, L. J. (2005). *J. Opt. Soc. Am. B*, *22*, 1681.
[2] Vella, A., Setaro, A., Piccirillo, B., & Santamato, E. (2003). *Phys. Rev. E*, *67*, 051704.
[3] Rosenblum, M. G., Pikovsky, A. S., & Kurths, J. (1996). *Phys. Rev. Lett.*, *76*, 1804.
[4] Pikovsky, A., Rosenblum, M., & Kurths, J. (2003). *Synchronization: A Universal Concept in Nonlinear Sciences*, Cambridge University Press: Cambridge.
[5] Lai, Y.-C., Armbruster, D., & Kostelich, E. J. (2000). *Phys. Rev. E*, *62*, R29; Pikovsky, A. and Rosenblum, M. (2001). *Phys. Rev. E*, *64*, 058203; Lai, Y.-C., Armbruster, D., & Kostelich, E. J. (2001). *Phys. Rev. E 64*, 058204.
[6] Brasselet, E., Doyon, B., Galstian, T. V., & Dubé, L. J. (2004). *Phys. Rev. E*, *69*, 021701.
[7] Durbin, S. D., Arakelian, S. M., & Shen, Y. R. (1981). *Opt. Lett.*, *6*, 411.
[8] Brasselet, E., Galstian, T. V., Dubé, L. J., Krimer, D. O., & Kramer, L. (2005). *J. Opt. Soc. Am. B*, *22*, 1671.
[9] Kantz, H. & Schreiber, T. (2004). *Nonlinear Time Series Analysis*, Cambridge University Press: Cambridge, 2nd ed.
[10] Schreiber, T. (1993). *Phys. Rev. E*, *47*, 2401.
[11] Rosenstein, M. T., Collins, J. J., & Luca, C. J. D. (1993). *Physica, D*, *65*, 117.
[12] Kantz, H. (1994). *Phys. Lett. A*, *185*, 77.
[13] Cipparrone, G., Carbone, V., Versace, C., Umeton, C., Bartolino, R., & Simoni, F. (1993). *Phys. Rev. E*, *47*, 3741.
[14] Russo, G., Carbone, V., & Cipparrone, G. (2000). *Phys. Rev. E*, *62*, 5036.
[15] Piccirillo, B., Toscano, C., Vetrano, F., & Santamato, E. (2001). *Phys. Rev. Lett.*, *86*, 2285.

[16] Brasselet, E., Lherbier, A., & Dubé, L. J. (2006). *J. Opt. Soc. Am. B*, *23*, 36.
[17] Zolot'ko, A. S., Kitaeva, V. F., Kuyumchyan, V. A., Sobolev, N. N., Sukhorukov, A. P., & Csillag, L. (1982). *Pis'ma Zh. Eksp. Teor. Fiz. 36*, 66 [JETP Lett. *36*, 80–84 (1982)].
[18] Brasselet, E. & Dubé, L. J. (2006). *Phys. Rev. E*, *73*, 021704.
[19] Kuramoto, Y. (1975). In: *International Symposium on Mathematical Problems in Theoretical Physics*, Araki, H. (Ed.), Lecture Notes in Physics No. 30, Springer: New York, 420.
[20] Matthews, P. C. & Strogatz, S. H. (1990). *Phys. Rev. Lett.*, *65*, 1701.
[21] Demeter, G., Krimer, D. O., & Kramer, L. (2005). *Phys. Rev. E*, *72*, 051712.